

A Simple Analytical Model for Rocky Planet Interiors

Li Zeng^{1,a} and Stein B. Jacobsen^{1,b}

¹*Department of Earth and Planetary Sciences, Harvard University, Cambridge, MA 02138*

^aastrozeng@gmail.com

^bjacobsen@neodymium.harvard.edu

ABSTRACT

This work aims at exploring the scaling relations among rocky exoplanets. With the assumption of internal gravity increasing linearly in the core, and staying constant in the mantle, and tested against numerical simulations, a simple model is constructed, applicable to rocky exoplanets of core mass fraction (CMF) $\in 0.1 \sim 0.4$ and mass $\in 0.1 \sim 10M_{\oplus}$. Various scaling relations are derived: (1) core radius fraction $\text{CRF} \approx \sqrt{\text{CMF}}$, (2) Typical interior pressure $P_{\text{typical}} \sim g_s^2$ (surface gravity squared), (3) core formation energy $E_{\text{diff}} \sim \frac{1}{10}E_{\text{grav}}$ (the total gravitational energy), (4) effective heat capacity of the mantle $C_p \approx \left(\frac{M_p}{M_{\oplus}}\right) \cdot 7 \cdot 10^{27}$ J K⁻¹, and (5) the moment of inertia $I \approx \frac{1}{3} \cdot M_p \cdot R_p^2$. These scaling relations, though approximate, are handy for quick use owing to their simplicity and lucidity, and provide insights into the interior structures of rocky exoplanets. As examples, this model is applied to several planets including Earth, GJ 1132b, Kepler-93b, and Kepler-20b, and made comparison with the numerical method.

Subject headings: Earth - planets and satellites: composition - planets and satellites: fundamental parameters - planets and satellites: interiors - planets and satellites: terrestrial planets

1. Introduction

Masses and radii of rocky exoplanets have been found for about a dozen cases (Figure 1), including Kepler-21b (Howell et al. 2012; Lopez-Morales et al. 2016), Kepler-20b (Gautier et al. 2012; Buchhave et al. 2016), COROT-7b (Leger et al. 2009; Queloz et al. 2009; Hatzes et al. 2011; Wagner et al. 2012; Haywood et al. 2014; Barros et al. 2014), HD219134b (Vogt et al. 2015; Motalebi et al. 2015), Kepler-10b (Batalha et al. 2011; Wagner et al. 2012; Dumusque et al.

2014; Esteves et al. 2015), Kepler-93b (Ballard et al. 2014; Dressing et al. 2015), Kepler-36b (Carter et al. 2012; Morton et al. 2016), Kepler-78b (Pepe et al. 2013; Grunblatt et al. 2015), K-105c (Rowe et al. 2014; Holczer et al. 2016; Jontof-Hutter et al. 2016), GJ 1132b (Berta-Thompson et al. 2015; Schaefer et al. 2016), and more are likely. Here we explore what other parameters can be further gleaned from this information. Our earlier work (Zeng et al. 2016) shows that by using an equation of state (EOS) for Earth for different core mass fractions (CMFs), a simple relationship between CMF, planetary radius, and mass can be found as

$$\text{CMF} = \frac{1}{0.21} \cdot \left[1.07 - \left(\frac{R_p}{R_\oplus} \right) / \left(\frac{M_p}{M_\oplus} \right)^{0.27} \right] \quad (1)$$

This work shows that the CMF can be related to the core radius fraction (CRF) of a rocky planet. A simple structural model can be calculated, which depends only on three parameters, (1) surface gravity g_s , (2) planet radius R_p , and (3) core radius fraction CRF. The procedure is as follows:

1. Surface gravity $g_s = \frac{G \cdot M_p}{R_p^2}$ can be calculated from mass M_p and radius R_p of a rocky planet, or directly from combining transiting depth with radial-velocity amplitude (Equation (16)).
2. CMF can be determined from Equation (1).
3. CRF can be estimated as $\sqrt{\text{CMF}}$.

The only assumption of this model is that the internal gravity profile can be approximated as a piecewise function (see Figure 2 Panel (1)a-d):

1. In the core, the gravity g increases linearly with radius from 0 at the center to g_s (surface value) at the core-mantle boundary (CMB): $g_{\text{core}}(r) = g_s \cdot \left(\frac{r}{R_{\text{core}}} \right) \propto r$
2. In the mantle, g stays constant: $g_{\text{mantle}}(r) = g_s = \text{const}$

This assumption is equivalent to assuming constant core density, followed by the mantle density decreasing to $\frac{2}{3}$ of the core density at CMB, and density decreasing as $\frac{1}{r}$ in the mantle.

The validity of this assumption is tested against the numerical results from solving the planetary structures with realistic EOS derived from PREM (Dziewonski & Anderson 1981), across the mass-radius range of $0.1 \sim 10 M_\oplus$ and $0.1 \lesssim \text{CMF} \lesssim 0.4$ for two-layer (core+mantle)

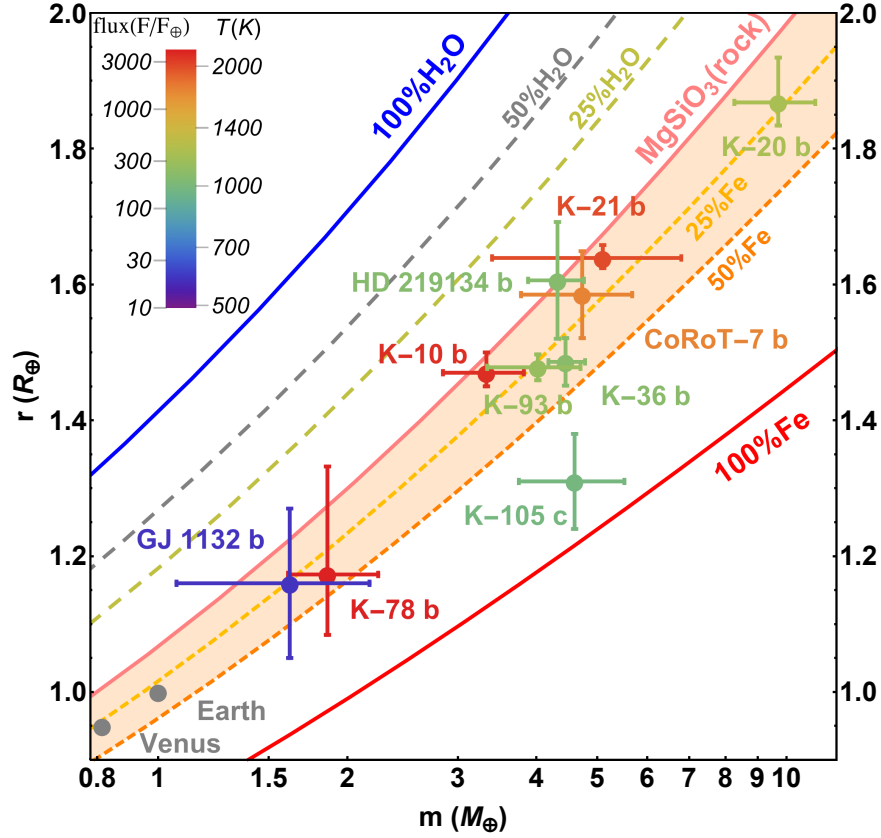


Fig. 1.— Mass-radius plot showing selected rocky planets. Curves show models of different compositions, with solid indicating single composition (Fe, $MgSiO_3$, i.e. rock, H_2O) and dashed indicating Mg-silicate planets with different amounts of H_2O or Fe added. Rocky planets without volatile envelope likely lie in the shaded region within uncertainty, and those ones with volatile envelope may lie above. Planets are color-coded by their incident bolometric stellar flux (compared to the Earth) and equilibrium temperatures assuming (1) circular orbit (2) uniform surface temperature (3) bond albedo $A=0$. Earth and Venus are shown for reference.

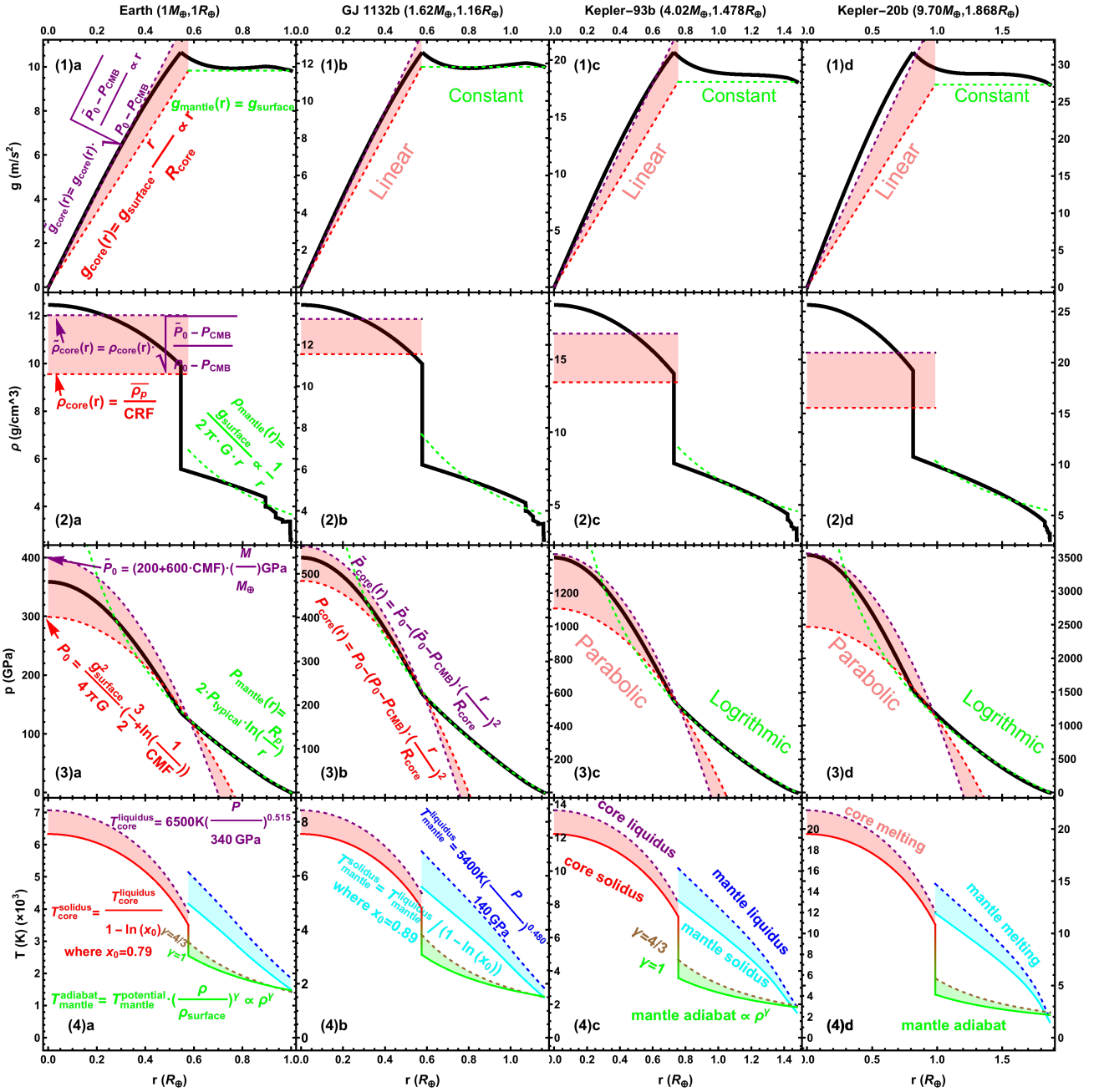


Fig. 2.— Numerical calculations based on PREM-extrapolated EOS (black) versus simple analytical models: Core (red, purple, and pink-area in between) and Mantle (green). Panel (1-4)a: Earth, Panel (1-4)b: GJ 1132b, Panel (1-4)c: Kepler-93b, Panel (1-4)d: Kepler-20b. Panel (1)a-d: Gravity Profiles (core is proportional to r and mantle is constant). Panel (2)a-d: Density Profiles (core is constant and mantle is inversely proportional to r). Panel (3)a-d: Pressure Profiles (core is parabolic in r and mantle is logarithmic in r). Panel (4)a-d: Temperature Profiles (best estimates shall lie in the green area (mantle) and pink area (core)). The solidus (where mixture starts to melt) and liquidus (where mixture completely melts) are plotted for comparison.

rocky planets. Note that Mercury lies outside this range of the CMF as it has a big core, owing to its likely giant impact origin (Asphaug & Reufer 2014).

Various scaling relations are derived from this model.

2. Scaling Relation between Pressure and Gravity

The two first-order differential equations (Seager et al. 2007; Zeng & Seager 2008; Zeng & Sasselov 2013) governing rocky planet interiors are

1. a hydrostatic equilibrium (force balance) equation:

$$\frac{dP}{dr} = -\frac{Gm\rho}{r^2} = -g \cdot \rho \quad (2)$$

2. a mass conservation equation:

$$\frac{dm}{dr} = 4\pi r^2 \rho \quad (3)$$

Equations (2) and (3) can be combined to give a relation between the internal pressure P and the mass m (mass contained within radius r , now used as the independent variable instead):

$$\frac{dP}{dm} = -\frac{Gm}{4\pi r^4} = -\frac{1}{4\pi G} \cdot \frac{g^2}{m} = -\frac{1}{4\pi G} \cdot g^2 \cdot \frac{d \ln(m)}{dm} \quad (4)$$

Integrating Equation (4), we get ($\ln(m)$ stands for the natural logarithmic of m)

$$\boxed{\int_{\text{surface}}^{\text{interior}} dP = -\frac{1}{4\pi G} \int_{M_p}^{\text{mass enclosed inside}} g^2 \cdot d \ln(m)} \quad (5)$$

This integration is from the surface inward, as the pressure at the surface is zero. Therefore, the typical internal pressure is on the order of

$$P \sim \frac{\overline{g^2}}{4\pi G} \quad (6)$$

where $\overline{g^2}$ is some average of g^2 . Defining planet mass as M_p , planet radius as R_p , and planet mean density as $\overline{\rho_p}$, then surface gravity g_s and characteristic interior pressure P_{typical} are

$$g_s \equiv \frac{GM_p}{R_p^2} \quad (7)$$

$$P_{\text{typical}} \equiv \frac{g_s^2}{4\pi G} = \frac{GM_p^2}{4\pi R_p^4} \quad (8)$$

P_{typical} will be shown to approximate P_{CMB} (pressure at CMB) later on. Given g_s in S.I. units (m s^{-2}) and pressures in GPa:

$$\boxed{P_{\text{CMB}} \sim P_{\text{typical}} \sim g_s^2} \quad (9)$$

For example, g_{\oplus} (Earth’s gravity) $\approx 10 \text{m s}^{-2}$, and $g_{\oplus}^2 \approx 100$ is near $P_{\oplus, \text{CMB}} = 136 \text{ GPa}$. The values of other planets are listed in Table 1.

3. Density Profile

Based on the assumption of the gravity profile, the density profile is

$$\rho_{\text{core}}(r) = \frac{3g_s}{4\pi GR_{\text{core}}} = \frac{\bar{\rho}_p}{\text{CRF}} = \text{constant, thus, } m_{\text{core}}(r) \propto r^3 \quad (10a)$$

$$\rho_{\text{mantle}}(r) = \frac{g_s}{2\pi Gr} \propto \frac{1}{r}, \text{ thus, } m_{\text{mantle}}(r) \propto r^2 \quad (10b)$$

Figure 2 Panel (2)a-d compares this to the PREM-derived density profiles. The $\frac{1}{r}$ dependence approximates the compression of mantle material toward depth, and the smaller core (CMF $\lesssim 0.4$) allows the core density to be approximated as constant. Generally, Equation (10a) approximates the density of the core near the CMB. Anywhere in the mantle,

$$\frac{m}{M_p} = \left(\frac{r}{R_p}\right)^2 \quad (11)$$

In particular, at the CMB,

$$\text{CMF} = \frac{M_{\text{core}}}{M_p} = \left(\frac{R_{\text{core}}}{R_p}\right)^2 = \text{CRF}^2 \quad (12)$$

In reality, this exact relation (Equation (12)) becomes approximate:

$$\boxed{\text{CRF} \approx \sqrt{\text{CMF}}} \quad (13)$$

The error of Equation (13) is generally within $\sim 10\%$ (see Table (1)). It is a quick way to estimate the CRF from the CMF and vice versa. It can even be applied to a rocky planet with a volatile envelope if it is only applied to the solid portion of that planet.

Table 1: Calculated parameters for four planets from this simple analytical model

	Earth	GJ 1132b	Kepler-93b	Kepler-20b
$M(M_{\oplus})$	1	1.62	4.02	9.70
$R(R_{\oplus})$	1	1.16	1.478	1.868
CMF (Equation (1))	0.33	0.25	0.26	0.28
CMF_N^1	0.32	0.27	0.28	0.22
CRF (Equation (13))	0.58	0.50	0.51	0.53
CRF_N	0.55	0.49	0.49	0.44
$\overline{\rho_p}(\text{g cm}^{-3})$	5.5	5.7	6.9	8.2
$g_s(\text{m s}^{-2})$ (Equation (7))	9.8	12	18	27
$P_{\text{typical}}(\text{TPa}^2)$ (Equation (8))	0.12	0.17	0.4	0.9
$P_{\text{CMB}}(\text{TPa})$ (Equation (15))	0.13	0.23	0.5	1.1
$P_0(\text{TPa})$ (Equation (22))	0.3	0.5	1.1	2.5
$\widetilde{P}_0(\text{TPa})$ (Equation (23))	0.40	0.56	1.4	3.6
$E_{\text{grav}}(10^{32}\text{J})$ (Equation (27))	2.4	5.6	27	120
$E_{\text{diff}}(10^{32}\text{J})$ (Equation (28)(29))	0.2	0.5	2.4	11
$E_{\text{mantle}}^{\text{thermal}}(10^{32}\text{J})$ (Equation (33)(34))	0.1	0.2	0.5	1.1
$T_{\text{mp}}(10^3\text{K})$	1.6	1.6	1.6	1.6
$T_{\text{mantle}}^{\text{CMB}}(10^3\text{K})$	2.5	3.1	3.6	4.1
$T_{\text{core}}^{\text{CMB}}(10^3\text{K})$	4	5	8	11
$T_{\text{center}}(10^3\text{K})$	6	7	12	20
$I(10^{38}\text{kg m}^2)$ (Equation (39)(40))	0.8	1.8	7.2	28

4. Pressure Profile

4.1. Pressure in the Mantle

Integrating Equation (5) with constant mantle gravity, we obtain

¹N stands for numerical simulation using **ManipulatePlanet** at astrozeng.com

²TPa = 1000 GPa = 10^{12} GPa.

$$P_{\text{mantle}}(m) = \frac{g_s^2}{4\pi G} \cdot \ln\left(\frac{M_p}{m}\right) = P_{\text{typical}} \cdot \ln\left(\frac{M_p}{m}\right) = 2P_{\text{typical}} \cdot \ln\left(\frac{R_p}{r}\right) \quad (14)$$

Evaluating Equation (14) at the CMB gives P_{CMB} (pressure at the CMB):

$$\boxed{P_{\text{CMB}} = P_{\text{typical}} \cdot \ln\left(\frac{1}{\text{CMF}}\right) = \frac{g_s^2}{4\pi G} \cdot \ln\left(\frac{1}{\text{CMF}}\right)} \quad (15)$$

For $\text{CMF} \in 0.1 \sim 0.4$, $P_{\text{CMB}} \in (0.9 \sim 2.3)P_{\text{typical}}$.

P_{CMB} is an important physical parameter, as it determines the state of core and mantle materials in contact. Equation (15) only depends on g_s and CMF. And g_s can be determined independent of the stellar parameters (Southworth et al. 2007) as

$$g_s = \frac{2\pi}{P_{\text{orb}}} \frac{(1 - e^2)^{1/2} A_{\text{RV}}}{(R/a)^2 \text{Sin}[i]} \quad (16)$$

where semi-amplitude A_{RV} and orbital eccentricity e can be constrained from the radial-velocity curve, and R/a is the radius over the semi-major axis ratio, which could be constrained directly from the transit light curve. The orbital period P_{orb} can be constrained from both. Thus, it is possible to estimate P_{CMB} even without knowing the accurate mass and radius in some cases for rocky planets.

4.2. Range of Applicability of This Model

From a theoretical point, we explore the range of applicability of this model.

Bulk modulus $K \equiv \frac{\partial P}{\partial \ln(\rho)}$. Therefore, in the mantle,

$$K_{\text{mantle}} = \frac{\partial P_{\text{mantle}}}{\partial \ln(\rho_{\text{mantle}})} = \frac{g_s^2}{4\pi G} \cdot \frac{d \ln(m)}{d \ln(r)} = 2 \cdot P_{\text{typical}} \quad (17)$$

Thus, in this model, the bulk modulus is constant everywhere in the mantle, equal to twice the typical internal pressure P_{typical} . Realistically, K shall increase with pressure, so how good is this approximation?

For Earth, $P_{\oplus, \text{typical}} = \frac{g_{\oplus}^2}{4\pi G} = 115$ GPa, so $K_{\oplus, \text{mantle}} = 230$ GPa. Comparing it to the

isentropic bulk modulus K_s of Earth's mantle according to PREM:
$$\begin{cases} K_{\oplus,LID} = 130 \text{ GPa} \\ K_{\oplus,670km} = 255.6 \sim 300 \text{ GPa} \\ K_{\oplus,D''} = 640 \text{ GPa} \end{cases}$$

So $K_{\oplus,mantle}$ represents the midrange of the realistic bulk modulus in the mantle. For higher masses, let us invoke the BM2 (Birch-Murnaghan second-order) EOS (Birch 1947, 1952), which when fitted to PREM gives $K_0 \approx 200\text{GPa}$ for both core and mantle (Zeng et al. 2016):

$$P = \frac{3}{2} \cdot K_0 \left[\left(\frac{\rho}{\rho_0} \right)^{\frac{7}{3}} - \left(\frac{\rho}{\rho_0} \right)^{\frac{5}{3}} \right] \quad (18)$$

Again, K is obtained by differentiating Equation (18):

$$K \equiv \frac{\partial P}{\partial \ln(\rho/\rho_0)} = \frac{3}{2} \cdot K_0 \left[\frac{7}{3} \cdot \left(\frac{\rho}{\rho_0} \right)^{\frac{7}{3}} - \frac{5}{3} \cdot \left(\frac{\rho}{\rho_0} \right)^{\frac{5}{3}} \right] \quad (19)$$

Equation (19) suggests: $\begin{cases} \text{when } P \lesssim K_0, K \approx K_0 \\ \text{when } P \gg K_0, K \rightarrow \frac{7}{3}P \approx 2P \end{cases}$. Since P_{typical} is the typical pressure in the mantle, $K \approx 2P \approx 2P_{\text{typical}}$. It is the same as Equation (17). Therefore, this approximation shall exist for higher masses as long as BM2 EOS holds. BM2 EOS's validity range extends above $10 M_{\oplus}$, and here we set the upper limit to be $10 M_{\oplus}$.

4.3. Pressure in the Core

Since $\rho_{\text{core}} = \text{constant}$ in this approximation, from Equation (2) we have

$$\frac{dP_{\text{core}}(r)}{dr} = -\frac{G}{r^2} \cdot \left(\frac{g_s}{GR_{\text{core}}} r^3 \right) \cdot \left(\frac{3g_s}{4\pi GR_{\text{core}}} \right) = -\frac{3r}{R_{\text{core}}^2} \cdot P_{\text{typical}} \quad (20)$$

Integrating it gives the pressure dependence on the radius as a parabolic function:

$$P_{\text{core}}(r) = P_0 - \frac{3}{2} \cdot P_{\text{typical}} \cdot \left(\frac{r}{R_{\text{core}}} \right)^2 \quad (21)$$

P_0 (central pressure) can be determined by connecting Equation (21) at CMB to P_{CMB} from Equation (15) as

$$P_0 = P_{\text{CMB}} + \frac{3}{2}P_{\text{typical}} = P_{\text{typical}} \cdot \left[\ln \left(\frac{1}{\text{CMF}} \right) + \frac{3}{2} \right] \Rightarrow P_0 \in (2.4 \sim 3.8) \cdot P_{\text{typical}} \quad (22)$$

Therefore, in this approximation, the pressure dependence on the radius is piecewise: parabolic in the core (Equation (21)) and logarithmic in the mantle (Equation (14)), and they interconnect at CMB. This piecewise pressure profile can be closely matched to the realistic pressure profile calculated from PREM as shown in Figure 2 Panel (3)a-d. Equation (22) tends to significantly underestimate the P_0 towards higher mass and higher CMF due to significant core compression. The following semi-empirical formula (Equation (23)) corrects this effect. Tested against numerical simulations, it gives a better estimate of P_0 to within $\sim 10\%$ error in the range of $\text{CMF} \in 0.1 \sim 0.4$ and $\text{mass} \in 0.1 \sim 10M_{\oplus}$.

$$\boxed{\widetilde{P}_0 \approx (200 + 600 \cdot \text{CMF}) \cdot \left(\frac{M_{\text{p}}}{M_{\oplus}} \right) \text{ GPa}} \quad (23)$$

A better approximation for the core pressure profile using \widetilde{P}_0 from Equation (23) and P_{CMB} from Equation (15), shown as the purple curves in Figure 2 Panel (3)a-d, is

$$\widetilde{P}_0(r) = \widetilde{P}_0 - (\widetilde{P}_0 - P_{\text{CMB}}) \cdot \left(\frac{r}{R_{\text{core}}} \right)^2 \quad (24)$$

The corrected core gravity $\widetilde{g}_{\text{core}}(r)$, shown as purple curves in Figure 2 Panel (1)a-d, and the corrected core density $\widetilde{\rho}_{\text{core}}$, shown as the purple curves in Figure 2 Panel (2)a-d, can be calculated as from \widetilde{P}_0 as

$$\frac{\widetilde{g}_{\text{core}}(r)}{g_{\text{core}}(r)} = \frac{\widetilde{\rho}_{\text{core}}}{\rho_{\text{core}}} = \sqrt{\left(\frac{\widetilde{P}_0 - P_{\text{CMB}}}{P_0 - P_{\text{CMB}}} \right)} \quad (25)$$

$\widetilde{\rho}_{\text{core}}$ from Equation (25) tends to better approximates the core density near the center, while ρ_{core} from Equation (10a) approximates the core density near the CMB.

5. Energy of Core Formation

The energy of core formation can be estimated as the difference in gravitational energies between the uniform-density state and this simple analytical model. According to the Virial

Theorem (Haswell 2010), the total gravitational energy is

$$E_{\text{grav}} = -3 \int_{\text{center}}^{\text{surface}} \frac{P}{\rho} \cdot dm \quad (26)$$

With the analytic forms of P and ρ in this model, Equation (26) can be integrated to obtain

$$E_{\text{grav}} = -\frac{GM_{\text{p}}^2}{3R_{\text{p}}} \cdot \left(2 - \frac{1}{5} \cdot \text{CRF}^3\right) \quad (27)$$

Comparing it to the gravitational energy of a uniform-density sphere, $E_{\text{grav, uniform sphere}} = -\frac{3}{5} \frac{GM_{\text{p}}^2}{R_{\text{p}}}$, the difference of the two can be regarded as the energy released during core formation (gravitational energy released from the concentration of denser materials toward the center):

$$E_{\text{diff}} = E_{\text{grav, uniform sphere}} - E_{\text{grav}} = \frac{GM_{\text{p}}^2}{R_{\text{p}}} \left(\frac{1}{15}(1 - \text{CRF}^3)\right) = \frac{GM_{\text{p}}^2}{R_{\text{p}}} \left(\frac{1}{15}(1 - \text{CMF}^{3/2})\right) \quad (28)$$

Since $\text{CMF} \in 0.1 \sim 0.4$, the term $\text{CMF}^{3/2}$ is small enough to be dropped to give

$$\boxed{E_{\text{diff}} \approx \frac{1}{15} \frac{GM_{\text{p}}^2}{R_{\text{p}}} \approx \frac{1}{10} |E_{\text{grav}}|} \quad (29)$$

Therefore, the energy released during core formation is $\sim 10\%$ of the total gravitational energy of such a rocky planet. For Earth, $E_{\text{diff}, \oplus} \approx 2.5 * 10^{31}$ J. The calculated values of other planets are listed in Table 1.

6. Thermal Content of the Planet

Since the temperatures inside the mantle of such a planet are likely above the Debye temperature of the solid, the heat capacity per mole of the atoms can be approximated as $3R$ (gas constant $R = 8.314 \text{ J K}^{-1} \text{ mol}^{-1}$). The specific heat capacity (heat capacity per unit mass) is $3R/\mu$ where μ is the average atomic weight of the composition, which for Mg-silicates (MgO , SiO_2 , or any proportion of them combined, such as MgSiO_3 or Mg_2SiO_4) is 0.02 kg mol^{-1} . The specific thermal energy u_{th} of the mantle material is thus

$$u_{\text{th}} = \frac{3RT}{\mu} \quad (30)$$

where T is temperature. The total thermal energy of mantle is calculated by the integration:

$$E_{\text{th,mantle}} = \int_{M_{\text{core}}}^{M_{\text{p}}} u_{\text{th}} \cdot dm = M_{\text{p}} \cdot \int_{\text{CMF}}^1 u_{\text{th}} \cdot dx \quad (31)$$

where $x \equiv \frac{m}{M_{\text{p}}}$. In this model, the mantle density $\rho_{\text{mantle}} \propto \frac{1}{r} \propto \frac{1}{\sqrt{m}}$ (Equation (10b)). On the other hand, with the assumption of the adiabatic temperature gradient in the mantle and the introduction of the Grüneisen parameter $\gamma \equiv \left. \frac{\partial \ln(T)}{\partial \ln(\rho)} \right|_{\text{adiabat}}$, the specific thermal energy can be rewritten to show its functional dependence on density ρ or mass m (Zeng & Jacobsen 2016):

$$u_{\text{th}} = \frac{3R \cdot T_{\text{mp}}}{\mu} \cdot \left(\frac{\rho}{\rho_0} \right)^\gamma = \frac{3R \cdot T_{\text{mp}}}{\mu} \cdot \left(\frac{m}{M_{\text{p}}} \right)^{-\frac{\gamma}{2}} \quad (32)$$

where T_{mp} (mantle potential temperature) is defined as the temperature where the mantle adiabat is extrapolated to zero pressure. For silicates, $\gamma \sim 1$, then,

$$E_{\text{th,mantle}} = 2 \cdot M_{\text{p}} \cdot \frac{3R \cdot T_{\text{mp}}}{\mu} (1 - \sqrt{\text{CMF}}) \quad (33)$$

For $\text{CMF} \approx 0.3$, $\sqrt{\text{CMF}} \approx \text{CRF} \approx 0.5$, and the total thermal energy of the mantle (considering only vibrations of the atoms in crystal lattices, while neglecting the electron contribution) is

$$E_{\text{th,mantle}} \approx \frac{3R \cdot T_{\text{mp}}}{\mu} \cdot M_{\text{p}} \approx \left(\frac{T_{\text{mp}}}{1000\text{K}} \right) \cdot \left(\frac{M_{\text{p}}}{M_{\oplus}} \right) \cdot 7 \cdot 10^{30} \text{ J} \quad (34)$$

Equation (34) suggests that concerning the thermal content, the mantle can be treated as an uncompressed mass of M_{p} at isothermal temperature of T_{mp} . Therefore, an effective heat capacity $C_{\text{th,mantle}}$ of the mantle can be defined with respect to T_{mp} :

$$C_{\text{th,mantle}} \approx \frac{3R}{\mu} \cdot M_{\text{p}} \approx \left(\frac{M_{\text{p}}}{M_{\oplus}} \right) \cdot 7 \cdot 10^{27} \text{ J K}^{-1} \quad (35)$$

The detailed calculation in Stacey & Davis (2008) shows that the effective heat capacity of the Earth's mantle is $7.4 \cdot 10^{27} \text{ J K}^{-1}$, indeed close to our estimate. Since the core is smaller

in comparison ($\text{CMF} \in 0.1 \sim 0.4$) and the core material has smaller specific heat capacity than silicates, the thermal content of the core should be generally less than that of the mantle. The mantle shall dictate the cooling of the core (Stacey & Davis 2008). Therefore, the mantle heat capacity can be regarded as an approximation for the total heat capacity of a planet.

Due to a feedback mechanism of silicate melting, there is good reason to set $T_{\text{mp}} \approx 1600$ K for Earth and super-Earths for a first approximation (Stixrude 2014). Then the temperature profiles inside these planets can be estimated using formulae in Stixrude (2014). The results are listed in Table 1 and plotted in Figure 2 Panel (4)a-d. In general, the mantle adiabat has shallower slope than the mantle melting curves (Zeng & Jacobsen 2016), so the mantle is mostly solid, while the core is partially or fully molten.

7. Moment of Inertia

The moment of inertia is calculated from Equation (36), where x represents the distance of the mass element to the rotational axis and the integration is over the entire volume (V):

$$I = \iiint_V x^2 \cdot \rho(\vec{r}) \cdot dV \quad (36)$$

Considering two simple cases:

$$\begin{cases} \text{thin spherical shell with radius } R_p, I_{\text{shell}} = \frac{2}{3}MR_p^2 \\ \text{uniform solid sphere with radius } R_p, I_{\text{solid sphere}} = \frac{2}{5}MR_p^2 \end{cases}$$

Defining $C \equiv I/MR_p^2$ as the moment-of-inertia factor, for shell $C = \frac{2}{3}$, and for sphere $C = \frac{2}{5}$. Smaller C corresponds to the mass being more concentrated toward the center. For this model, the moment of inertia of the core and the mantle can each be calculated separately, then combined to give the total moment of inertia of the planet:

$$I_{\text{core}} = \frac{2}{5}M_p R_p^2 \cdot \text{CMF}^2 \quad (37)$$

$$I_{\text{mantle}} = \frac{1}{3}M_p R_p^2 \cdot (1 - \text{CMF}^2) \quad (38)$$

$$I_{\text{total}} = I_{\text{core}} + I_{\text{mantle}} = \frac{1}{3}M_p R_p^2 \cdot \left(1 + \frac{1}{5} \cdot \text{CMF}^2\right) \quad (39)$$

Considering $CMF \in 0.1 \sim 0.4$, the term $\frac{1}{5}CMF^2$ can be ignored, so $C \approx \frac{1}{3}$. In the solar system, the C for Mercury, Venus, and Earth is indeed very close to $\frac{1}{3}$ (Rubie et al. 2007). Here we show that $C \approx \frac{1}{3}$ can be generalized to other rocky exoplanets:

$$\boxed{I_{\text{planet}} \approx \frac{1}{3} \cdot M_p \cdot R_p^2} \quad (40)$$

For Earth, $M_{\oplus}R_{\oplus}^2 = 2.4 \cdot 10^{38}$ kg m², and $I_{\oplus} \approx \frac{1}{3}M_{\oplus}R_{\oplus}^2 = 8 \cdot 10^{37}$ kg m². The angular momentum of Earth’s rotation is $L_{\oplus} = I_{\oplus} \cdot \Omega_{\oplus} = 6 \cdot 10^{33}$ kg m² s⁻¹. The total rotational energy of Earth is $E_{\text{rot}} = \frac{1}{2} \cdot I_{\oplus} \cdot \Omega_{\oplus}^2 = \frac{L_{\oplus}^2}{2 \cdot \Omega_{\oplus}^2} = 2 \cdot 10^{29}$ J, where $\Omega_{\oplus} = 7.3 \cdot 10^{-5}$ rad s⁻¹ is the angular frequency of Earth’s rotation. The calculated moment of inertia of other planets are shown in Table 1.

8. Conclusion

A simple analytical model for rocky planetary interiors is presented here and compared to numerical results. It explores the scaling relations among the following five aspects: (1) the relative size and mass of the core and the mantle, (2) the interior pressure and gravity, (3) the core formation energy and the gravitational energy, (4) the heat content and temperature profiles, and (5) the moment of inertia. Other results can be derived from this model.

Although being approximate, these results are straightforward to apply, as in many cases mass and radius are only measured approximately. Combined with the mass-radius relation, these formulae shall provide us with a new way of looking at the rocky planetary interiors, complementing the numerical approach.

9. Acknowledgement

This work was supported by a grant from the Simons Foundation (SCOL [award #337090] to L.Z.). The authors would like to thank Mr. and Mrs. Simons and the Simons Foundation for generously supporting this research project. The author L.Z. would like to thank his father Lingwei Zeng and mother Ling Li for continuous support and help. He also would like to thank Eugenia Hyung for insightful discussion of this paper. Part of this research was also conducted under the Sandia Z Fundamental Science Program and supported by the Department of Energy National Nuclear Security Administration under Award Numbers DE-NA0001804 and DE-NA0002937 to S.B.J (PI) with Harvard University. This research

reflects the authors' views and not those of the DOE. Finally, the authors would like to thank Dimitar D. Sasselov for insightful suggestions and helpful comments on this paper.

REFERENCES

- Asphaug, E., & Reufer, A. 2014, *Nature Geoscience*, 7, 564
- Ballard, S., Chaplin, W. J., Charbonneau, D., et al. 2014, *The Astrophysical Journal*, 790, 12
- Barros, S. C. C., Almenara, J. M., Deleuil, M., et al. 2014, *A&A*, 569, A74
- Batalha, N. M., Borucki, W. J., Bryson, S. T., et al. 2011, *The Astrophysical Journal*, 729, 27
- Berta-Thompson, Z. K., Irwin, J., Charbonneau, D., et al. 2015, *Nature*, 527, 204
- Birch, F. 1947, *Physical Review*, 71, 809
- . 1952, *J. Geophys. Res.*, 57, 227
- Buchhave, L. A., Dressing, C. D., Dumusque, X., et al. 2016, *ApJ* accepted, arXiv:1608.06836
- Carter, J. A., Agol, E., Chaplin, W. J., et al. 2012, *Science*, 337, 556
- Dressing, C. D., Charbonneau, D., Dumusque, X., et al. 2015, *ApJ*, 800, 135
- Dumusque, X., Bonomo, A. S., Haywood, R. D., et al. 2014, *ApJ*, 789, 154
- Dziewonski, A. M., & Anderson, D. L. 1981, *Physics of the Earth and Planetary Interiors*, 25, 297
- Esteves, L. J., De Mooij, E. J. W., & Jayawardhana, R. 2015, *ApJ*, 804, 150
- Gautier, T. N., III, Charbonneau, D., et al. 2012, *The Astrophysical Journal*, 749, 15
- Grunblatt, S. K., Howard, A. W., & Haywood, R. D. 2015, *ApJ*, 808, 127
- Haswell, C. A. 2010, *Transiting Exoplanets* (Cambridge University Press)
- Hatzes, A. P., Fridlund, M., Nachmani, G., et al. 2011, *The Astrophysical Journal*, 743, 75
- Haywood, R. D., Collier Cameron, A., Queloz, D., et al. 2014, *MNRAS*, 443, 2517
- Holczer, T., Mazeh, T., Nachmani, G., et al. 2016, *ApJS*, 225, 9
- Howell, S. B., Rowe, J. F., Bryson, S. T., et al. 2012, *The Astrophysical Journal*, 746, 123
- Jontof-Hutter, D., Ford, E. B., Rowe, J. F., et al. 2016, *The Astrophysical Journal*, 820, 39

- Leger, A., Rouan, D., Schneider, J., et al. 2009, *Astronomy and Astrophysics*, 506, 287
- Lopez-Morales, M., Haywood, R. D., Coughlin, J. L., et al. 2016, ArXiv e-prints, arXiv:1609.07617
- Morton, T. D., Bryson, S. T., Coughlin, J. L., et al. 2016, *ApJ*, 822, 86
- Motalebi, F., Udry, S., Gillon, M., et al. 2015, ArXiv e-prints, arXiv:1507.08532
- Pepe, F., Cameron, A. C., Latham, D. W., et al. 2013, *Nature*, 503, 377
- Queloz, D., Bouchy, F., Moutou, C., Hatzes, A., & Hébrard, G. 2009, *Astronomy and Astrophysics*, 506, 303
- Rowe, J. F., Bryson, S. T., Marcy, G. W., et al. 2014, *ApJ*, 784, 45
- Rubie, D., Nimmo, F., & Melosh, H. 2007, in *Treatise on Geophysics*, ed. G. Schubert (Amsterdam: Elsevier), 51 – 90
- Schaefer, L., Wordsworth, R., Berta-Thompson, Z., & Sasselov, D. 2016, ArXiv e-prints, arXiv:1607.03906
- Seager, S., Kuchner, M., Hier-Majumder, C. A., & Militzer, B. 2007, *The Astrophysical Journal*, 669, 1279
- Southworth, J., Wheatley, P. J., & Sams, G. 2007, *MNRAS*, 379, L11
- Stacey, F. D., & Davis, P. M. 2008, *Physics of the Earth* by Frank D. Stacey and Paul M. Davis, fourth edition. 2008; ISBN: 978-0-521-87362-8 (hardback) (Cambridge University Press)
- Stixrude, L. 2014, *Philosophical Transactions of the Royal Society of London Series A*, 372, 20130076
- Vogt, S. S., Burt, J., Meschiari, S., et al. 2015, *ApJ*, 814, 12
- Wagner, F. W., Tosi, N., Sohl, F., Rauer, H., & Spohn, T. 2012, *A&A*, 541, A103
- Zeng, L., & Jacobsen, S. B. 2016, *The Astrophysical Journal*, 829, 18
- Zeng, L., & Sasselov, D. 2013, *Publications of the Astronomical Society of the Pacific*, 125, pp. 227
- Zeng, L., Sasselov, D. D., & Jacobsen, S. B. 2016, *ApJ*, 819, 127

Zeng, L., & Seager, S. 2008, *Publications of the Astronomical Society of the Pacific*, 120, 983